

Harmonic spectrum of pulsar timing array angular correlations

Bruce Allen*

Max Planck Institute for Gravitational Physics (Albert Einstein Institute),
Leibniz Universität Hannover, Callinstrasse 38, D-30167, Hannover, Germany

Joseph D. Romano†

Department of Physics and Astronomy, University of Texas Rio Grande Valley,
One West University Boulevard, Brownsville, TX 78520, USA

(Dated: December 20, 2024)

Pulsar timing arrays (PTAs) detect gravitational waves (GWs) via the correlations they create in the arrival times of pulses from different pulsars. The mean correlation, a function of the angle γ between the directions to two pulsars, was predicted in 1983 by Hellings and Downs (HD). Observation of this angular pattern is crucial evidence that GWs are present, so PTAs “reconstruct the HD curve” by estimating the correlation using pulsar pairs separated by similar angles. The angular pattern may be also expressed as a “harmonic sum” of Legendre polynomials $P_l(\cos \gamma)$, with coefficients c_l . Here, assuming that the GWs and pulsar noise are described by a Gaussian ensemble, we derive optimal estimators for the c_l and compute their variance. We consider two choices for “optimal”. The first minimizes the variance of each c_l , independent of the values of the others. The second finds the set of c_l which minimizes the (squared) deviation of the reconstructed correlation curve from its mean. These are analogous to the so-called “dirty” and “clean” maps of the electromagnetic and (audio-band) GW backgrounds.

Introduction.— This paper is about reconstruction of the Hellings and Downs (HD) correlation [1], starting from pulsar timing array (PTA) data [2–6]. Previous work [7] shows how to optimally estimate this correlation using data from a set of pulsar pairs lying in a particular angular separation bin [8]. This paper shows how to optimally reconstruct the correlation expressed in harmonic form, as a sum of Legendre polynomials, using all pulsar pairs.

This paper must be read in conjunction with [7], because we omit almost all equations which can be taken from there. Those are referred to using the notation (AR7) to indicate Eq. (7) of [7].

The goal is to reconstruct the HD correlation $-1 \leq \frac{3}{2}\mu \leq 1$ as a function of the angle $\gamma \in [0, \pi]$ between the directions to pulsars [7, Introduction]. The correlation can be expressed as a sum of Legendre polynomials

$$\mu(\gamma) = \sum_{l=0}^{\infty} c_l P_l(\cos \gamma). \quad (1)$$

Here, we derive optimal estimators for the c_l and compute their variance.

The expected value of the correlation is called the HD curve $\mu_u(\gamma) \equiv \langle \mu(\gamma) \rangle$ and is illustrated in Fig. 1. The corresponding expected values of the harmonic coefficients are computed in [9–11] and are

$$\langle c_l \rangle = \begin{cases} 0 & \text{for } l < 2 \\ (2l + 1) / ((l + 2)(l + 1)l(l - 1)) & \text{for } l \geq 2. \end{cases} \quad (2)$$

These different contributions are also shown in Fig. 1; partial sums may be seen in [12, Fig. 11]. Because the $\langle c_l \rangle$ fall off like $1/l^3$ for large l , summing the terms up

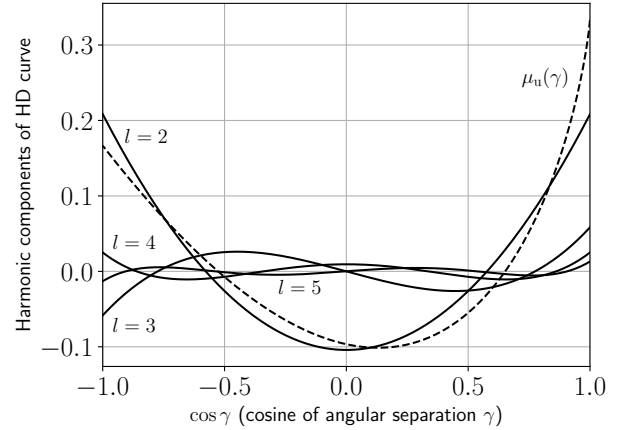


FIG. 1. The HD curve $\mu_u(\gamma)$ (dashed line) and its first four harmonic components $\langle c_l \rangle P_l(\cos \gamma)$ (solid lines).

to $l = 5$ already gives a good approximation of the HD curve. (Note that the correlation is doubled to $3\mu_u(0) = 1$ for pulsars that are closer together than the typical GW wavelength, see [13, App. C.2].)

Approach 1: Matched Filter – Our first approach is inspired by that of [7]. In (AR23) we considered estimators $\hat{\mu}(\gamma)$ which are arbitrary linear combinations of the form

$$\sum_{ab \in \gamma} \sum_{j,k} W_{ab}^{jk} Z_a^j Z_b^k, \quad (3)$$

where Z_a^j is the (complex) Fourier amplitude of the redshift of pulsar a in frequency bin j , defined in (AR12), and the W_{ab}^{jk} are a set of weights. There, the sum was over a set of pulsar pairs ab in a narrow angular bin at angle γ , and the weights satisfied $W_{ab}^{jk*} = W_{ab}^{-j,-k}$, to

ensures that the estimator is real. The weights were selected so that the estimator is unbiased and minimum variance. (Note that all analysis there and here may also be done in terms of timing residuals; the results are identical, see [7, Footnote 19].)

In analogy with this, we define an unbiased estimator for c_l . The estimator is analogous to (AR28), although we do not know how to derive it from first principles. For a PTA containing N_{pul} pulsars, the estimator is

$$\begin{aligned} \hat{c}_l &\equiv \langle c_l \rangle \frac{(\boldsymbol{\mu}_l \bar{\mathbf{H}})^t \mathbf{C}^{-1} \mathbf{Z} \mathbf{Z}}{(\boldsymbol{\mu}_l \bar{\mathbf{H}})^t \mathbf{C}^{-1} (\boldsymbol{\mu}_l \bar{\mathbf{H}})} \\ &\equiv \langle c_l \rangle \frac{\sum_{a < b} \sum_{c < d} \sum_{j, k} \sum_{\ell, m} \mu_{l, ab} \bar{H}_{jk} (C^{-1})_{ab, cd}^{jk, \ell m} Z_c^\ell Z_d^m}{\sum_{a < b} \sum_{c < d} \sum_{j, k} \sum_{\ell, m} \mu_{l, ab} \bar{H}_{jk} (C^{-1})_{ab, cd}^{jk, \ell m} \mu_{cd} \bar{H}_{\ell m}}, \end{aligned} \quad (4)$$

where $\mathbf{Z} \mathbf{Z} \equiv Z_a^j Z_b^k$. Here,

$$\boldsymbol{\mu}_l \equiv \mu_{l, ab} \equiv (1 + \delta_{ab}) P_l(\cos \gamma_{ab}). \quad (5)$$

and $\boldsymbol{\mu} = \sum_l \langle c_l \rangle \boldsymbol{\mu}_l$ are vectors of dimension $N_{\text{pair}} = N_{\text{pul}}(N_{\text{pul}} - 1)/2$. In contrast with (3), the sum is *not* confined to a particular angular bin, but includes *all possible* pulsar-pair cross-correlations $a < b$.

This estimator takes the form

$$\hat{c}_l = \langle c_l \rangle \frac{d_l}{u_l}, \quad (6)$$

where we have defined

$$d_l \equiv (\boldsymbol{\mu}_l \bar{\mathbf{H}})^t \mathbf{C}^{-1} \mathbf{Z} \mathbf{Z}, \quad (7)$$

$$u_l \equiv (\boldsymbol{\mu}_l \bar{\mathbf{H}})^t \mathbf{C}^{-1} (\boldsymbol{\mu}_l \bar{\mathbf{H}}). \quad (8)$$

Expression (7) is an *optimal matched filter* for the angular correlation pattern $\boldsymbol{\mu}_l$. The corresponding “filter template” (5) is proportional to the l ’th term in (1); the δ_{ab} can be dropped since $a < b$. This is an optimal matched filter because it is obtained by “whitening the template and the data” via the inverse covariance matrix \mathbf{C}^{-1} , and then normalizing. Our normalization, placing u_l in the denominator of (6), gives an unbiased estimator of c_l . To see this, note that $\langle \mathbf{Z} \mathbf{Z} \rangle = \boldsymbol{\mu} \bar{\mathbf{H}}$. It follows from inspection of (7) and (8) that $\langle d_l \rangle = u_l$, thus implying $\langle \hat{c}_l \rangle = \langle c_l \rangle$.

The variance of the optimal matched filter estimator (4) is easy to calculate. The covariance of $\mathbf{Z} \mathbf{Z}$ is

$$\mathbf{C} \equiv \langle \mathbf{Z} \mathbf{Z} (\mathbf{Z} \mathbf{Z})^\dagger \rangle - \langle \mathbf{Z} \mathbf{Z} \rangle \langle (\mathbf{Z} \mathbf{Z})^\dagger \rangle. \quad (9)$$

An explicit formula for $\mathbf{C} \equiv C_{ab, cd}^{jk, \ell m}$ is given in (AR19), in terms of covariance matrices computed from the gravitational wave background (GWB) and pulsar noise power spectra. The covariance matrix \mathbf{C} , whose inverse \mathbf{C}^{-1}

appears in (4), is the symmetric part of \mathcal{C} with respect to the frequency indices (AR20):

$$\mathbf{C} \equiv C_{ab, cd}^{jk, \ell m} \equiv C_{ab, cd}^{(jk), (\ell m)} \quad (10)$$

From the definition (7) of the d_l it follows that their covariance is

$$\begin{aligned} \langle d_l d_{l'} \rangle - \langle d_l \rangle \langle d_{l'} \rangle &= (\boldsymbol{\mu}_l \bar{\mathbf{H}})^t \mathbf{C}^{-1} (\langle (\mathbf{Z} \mathbf{Z}) (\mathbf{Z} \mathbf{Z})^\dagger \rangle - \langle \mathbf{Z} \mathbf{Z} \rangle \langle (\mathbf{Z} \mathbf{Z})^\dagger \rangle) \\ &\quad \times \mathbf{C}^{-1} (\boldsymbol{\mu}_{l'} \bar{\mathbf{H}}) \\ &= (\boldsymbol{\mu}_l \bar{\mathbf{H}})^t \mathbf{C}^{-1} \mathbf{C} \mathbf{C}^{-1} (\boldsymbol{\mu}_{l'} \bar{\mathbf{H}}) \\ &= F_{ll'}, \end{aligned} \quad (11)$$

where (9) was used to get the second equality and we have defined a matrix

$$\mathbf{F} \equiv F_{ll'} \equiv (\boldsymbol{\mu}_l \bar{\mathbf{H}})^t \mathbf{C}^{-1} (\boldsymbol{\mu}_{l'} \bar{\mathbf{H}}), \quad (12)$$

where l and l' are indices labeling harmonics. Thus, the variance of the HD correlation estimator is

$$\begin{aligned} \sigma_{\hat{c}_l}^2 &\equiv \langle \hat{c}_l^2 \rangle - \langle \hat{c}_l \rangle^2 \\ &= \langle c_l \rangle^2 (\langle d_l^2 \rangle - \langle d_l \rangle^2) / u_l^2 \\ &= \langle c_l \rangle^2 F_{ll} / u_l^2, \end{aligned} \quad (13)$$

where F_{ll} are the diagonal elements of \mathbf{F} .

We will write the variance (13) as

$$\sigma_{\hat{c}_l}^2 = \frac{\langle c_l \rangle^2}{(2L_{\text{eff}} + 1) N_{\text{freq}}} = \frac{\langle c_l \rangle^2 F_{ll}}{u_l^2}, \quad (14)$$

where N_{freq} and $2L_{\text{eff}} + 1$ are functions of l . (This, along with the formulas given below for N_{freq} and $2L_{\text{eff}} + 1$, is one of the two main results of this paper.) The division into the two factors is arbitrary; we break this degeneracy by imposing two requirements: (i) The effective number of frequency bins N_{freq} for which the GWB dominates pulsar noise equals N_{cr} in the crossover frequency limit. (ii) The effective number of harmonic degrees of freedom $2L_{\text{eff}} + 1$ depends only on the “geometry” of the pulsar timing array, meaning the pulsar sky directions. Note: the crossover frequency limit is discussed and defined in [7] between (AR34) and (AR35).

To find $2L_{\text{eff}} + 1$ and N_{freq} , we start with requirement (i), computing \mathbf{F} in the crossover frequency limit, where below “crossover” frequency N_{cr}/T , the GWB dominates the redshifts or timing residuals, and above that frequency, the pulsar noise dominates. In this crossover limit, $N_{\text{freq}} \rightarrow N_{\text{cr}}$. The spectrum H_{jk} of the GWB is nonzero only for frequency bins $|j|, |k| \leq N_{\text{cr}}$ and vanishes if either $|j|$ or $|k|$ is larger than N_{cr} . The pulsar spectrum P_a^{jk} has the opposite behavior. For this case, the inverse of the covariance matrix is given by (AR35). Since \mathbf{H} or $\bar{\mathbf{H}}$ contracted with \mathbf{P}_a vanishes, the same calculation as in (AR37) shows that

$$F_{ll'} \rightarrow 2N_{\text{freq}} \mathcal{G}_{ll'}, \quad u_l \rightarrow 2N_{\text{freq}} v_l, \quad (15)$$

where

$$\mathcal{G} \equiv \mathcal{G}_{ll'} \equiv (\boldsymbol{\mu}_l)^t \mathbf{G}^{-1} \boldsymbol{\mu}_{l'}, \quad (16)$$

$$v_l \equiv (\boldsymbol{\mu}_l)^t \mathbf{G}^{-1} \boldsymbol{\mu}. \quad (17)$$

Substituting these limiting expressions for F_{ll} and u_l into the rhs of (14) implies that

$$2L_{\text{eff}} + 1 \equiv \frac{2v_l^2}{\mathcal{G}_{ll}}. \quad (18)$$

While (18) was obtained in the crossover limit, requirement (ii) implies that it must always hold. It then follows from (14) and (18) that

$$N_{\text{freq}} \equiv \frac{1}{2} \frac{\mathcal{G}_{ll}}{F_{ll}} \left(\frac{u_l}{v_l} \right)^2 \quad (19)$$

holds in general (not just in the crossover limit). Note that N_{freq} depends upon the GWB and pulsar power spectra, as well as upon the pulsar sky positions and l .

The effective number of harmonic degrees of freedom $2L_{\text{eff}} + 1$ given by (18) simplifies when there are many pulsars uniformly distributed on the sky. To see this, we use results from [8], noting that the C_l as defined in [8, Eq. (4.14)] are related to the $\langle c_l \rangle$ as given in (2) by $\langle c_l \rangle = (2l + 1)C_l$. From [8, set $\hbar = 1$ in Eq. (4.25)] the many-pulsar-pair limit of $\mathbf{G}^{-1} \equiv (G^{-1})_{ab,cd}$ is proportional to

$$G^{-1}(x, x') = \frac{1}{8} \sum_{l=2}^{\infty} \frac{(2l+1)^3}{\langle c_l \rangle^2} P_l(x) P_l(x'), \quad (20)$$

where $x = \cos \gamma_{ab}$ and $x' = \cos \gamma_{cd}$, and it is understood that this denotes the average value over many pulsar pairs at a given angular separation. The discrete and continuous quantities and their inverses are related by [8, Eq. (4.29)]

$$\begin{aligned} G_{ab,cd} &= G(\cos \gamma_{ab}, \cos \gamma_{cd}) \\ (G^{-1})_{ab,cd} &= \left(\frac{2}{N_{\text{pair}}} \right)^2 G^{-1}(\cos \gamma_{ab}, \cos \gamma_{cd}). \end{aligned} \quad (21)$$

In the many-pulsar limit, $\frac{1}{N_{\text{pair}}} \sum_{a<b} \rightarrow \frac{1}{2} \int_{-1}^1 dx$. So, by using (5) and (16) one can see that $\mathcal{G}_{ll'}$ approaches

$$\begin{aligned} \mathcal{G}_{ll'} &\rightarrow \int_{-1}^1 dx \int_{-1}^1 dx' P_l(x) G^{-1}(x, x') P_{l'}(x') \\ &= \begin{cases} 0 & \text{if } l < 2 \\ \frac{2l+1}{2\langle c_l \rangle^2} \delta_{ll'} & \text{if } l \geq 2. \end{cases} \end{aligned} \quad (22)$$

To obtain the final equality above we have used (20) and the orthogonality relation

$$\int_{-1}^1 dx P_l(x) P_{l'}(x) = \frac{2}{2l+1} \delta_{ll'} \quad (23)$$

for the Legendre polynomials.

The diagonal form of \mathcal{G} in this many pulsar limit reflects the orthogonality of the different spherical harmonics when sampled very finely on the sphere. Note that in this limit \mathcal{G} vanishes along the first two rows and columns $l = 0, 1$ and $l' = 0, 1$. This is because \mathbf{G}^{-1} does not contain either of these harmonics, as can be seen from (20). It follows that in this limit, every entry of the pseudoinverse \mathcal{G}^{-1} of \mathcal{G} vanishes except for the diagonal elements starting in the third row/column, where $(\mathcal{G}^{-1})_{ll} = 1/\mathcal{G}_{ll}$ for $l \geq 2$.

We use a similar calculation to evaluate v_l in the many-pulsar limit. Starting from (17) gives

$$v_l \rightarrow \mathcal{G}_{ll} \langle c_l \rangle \rightarrow \frac{2l+1}{2\langle c_l \rangle} \quad \text{for } l \geq 2. \quad (24)$$

Inserting (22) and (24) into (18) implies that in the limit of many pulsars, uniformly distributed on the sky,

$$2L_{\text{eff}} + 1 \rightarrow \begin{cases} 0 & \text{for } l < 2 \\ 2l+1 & \text{for } l \geq 2. \end{cases} \quad (25)$$

In effect, with enough pulsars spread around the sky, all of the degrees of freedom of any multipole can be observed and measured. If not, then (18) is the effective number of degrees of freedom which could be observed with the given set, if enough SNR were available. Shown in Table I are the values of $2L_{\text{eff}} + 1$ for the pulsars used by the different pulsar timing arrays mentioned in the Introduction, along with a fictitious PTAs formed from the union of their pulsars, and larger numbers of randomly-placed pulsars.

Thus, in the many pulsar case, we obtain

$$\sigma_{c_l}^2 = \frac{\langle c_l \rangle^2}{(2l+1)N_{\text{freq}}}. \quad (26)$$

This is a generalization of the many-pulsar single-frequency-bin case considered by Roebber and Holder [10], which is obtained by setting $N_{\text{freq}} = 1$.

Approach 2: Best Fit – Our second approach differs from the first. There, the goal was to estimate a single c_l “in isolation”, without taking into consideration the values of the other $c_{l'}$ (for $l' \neq l$). Here, we will instead minimize a “global” quantity χ^2 that characterizes the difference between the observed correlations and the harmonic model (1). This strives to simultaneously find the best estimator for a set of c_l . We denote this set by $\mathbf{c} \equiv \{c_l\}$, with the understanding that this denotes some finite subset of $\{c_0, c_1, \dots\}$. (The remaining c_l may be set to zero or other fixed/definite values.)

The starting point of this \mathbf{c} “reconstruction” is a real quadratic function χ^2 of \mathbf{c} , defined by

$$\begin{aligned} \chi^2(\mathbf{c}) &\equiv \boldsymbol{\Delta}^t(\mathbf{c}) \mathbf{C}^{-1} \boldsymbol{\Delta}^*(\mathbf{c}) \\ &\equiv \sum_{a<b} \sum_{c<d} \sum_{j,k} \sum_{\ell,m} \Delta_{ab}^{jk}(\mathbf{c}) (\mathbf{C}^{-1})_{ab,cd}^{j\ell,km} \Delta_{cd}^{\ell m*}(\mathbf{c}), \end{aligned} \quad (27)$$

l	$2l+1$	EPTA 25		PPTA 30		CPTA 57		NG 67		IPTA3 115		All 127		RU 200		RU 300	
		$2L_e+1$		$2L_e+1$		$2L_e+1$		$2L_e+1$		$2L_e+1$		$2L_e+1$		$2L_e+1$		$2L_e+1$	
0	1	0.067	0	0.001	0	0.030	0	0.009	0	0.002	0	0.001	0	0.001	0	0	0
1	3	0.011	0	0.057	0	0.267	0	0.022	0	0.010	0	0.008	0	0.001	0	0	0
2	5	2.015	1.725	2.628	2.310	3.246	2.889	3.388	3.271	4.023	3.921	4.122	4.069	4.551	4.560	4.709	4.710
3	7	0.604	0.362	0.932	0.450	1.763	1.037	1.908	1.669	2.912	2.615	3.189	3.004	4.551	4.586	5.265	5.270
4	9	0.386	0.064	0.363	0.107	1.035	0.304	0.788	0.499	1.514	1.114	1.641	1.376	2.999	3.071	4.207	4.221
5	11	0.250	0.017	0.081	0.030	0.557	0.120	0.464	0.183	0.914	0.460	0.906	0.575	1.474	1.537	2.523	2.549
6	13	0.097	0.006	0.006	0.007	0.306	0.048	0.271	0.072	0.536	0.191	0.525	0.242	0.640	0.692	1.270	1.295
7	15	0.108	0.002	0.002	0.003	0.179	0.020	0.141	0.031	0.307	0.086	0.299	0.108	0.270	0.309	0.601	0.622
8	17	0.019	0.001	0.008	0.001	0.111	0.009	0.084	0.014	0.196	0.039	0.197	0.049	0.118	0.142	0.288	0.298
9	19	0.031	0.000	0.016	0.001	0.068	0.004	0.038	0.007	0.104	0.020	0.102	0.025	0.053	0.068	0.139	0.151
10	21	0.018	0.000	0.026	0.000	0.044	0.002	0.018	0.003	0.059	0.010	0.058	0.013	0.022	0.034	0.073	0.078
11	23	0.009	0.000	0.034	0.000	0.026	0.001	0.004	0.002	0.028	0.006	0.031	0.007	0.008	0.018	0.040	0.043
12	25	0.005	0.000	0.020	0.000	0.028	0.001	0.003	0.001	0.017	0.003	0.023	0.004	0.003	0.011	0.023	0.024

TABLE I. The effective number of observable angular degrees of freedom $2L_{\text{eff}} + 1$ for different PTAs, which are listed on the first row followed by the number of pulsars. In each entry, the first value is (18) for Approach 1, and the second value is (38) for Approach 2. (By definition, the latter vanish for $l < 2$.) The main sensitivity is to the first few harmonics beginning with $l = 2$. The ‘‘All’’ PTA includes all pulsars from the previous columns, eliminating duplicates. The final two columns show 200 and 300 pulsars placed randomly on the sky as a Random Uniform Poisson process.

where

$$\Delta(\mathbf{c}) \equiv \Delta_{ab}^{jk}(\mathbf{c}) \equiv Z_a^j Z_b^k - \bar{H}_{jk} \sum_{c_l \in \mathbf{c}} c_l \mu_{l,ab} \quad (28)$$

and \mathbf{C}^{-1} is the inverse of the covariance matrix given in (9). The Δ 's and the statistic χ^2 are measures of the difference between the observed spatial correlations and the model $\sum_l c_l \mu_{l,ab}$ of (1), restricted to $c_l \in \mathbf{c}$. The value of χ^2 is a function of the observed redshifts (or timing residuals), of the GWB and pulsar noise spectral models, and of a set of real coefficients \mathbf{c} .

In this approach, model selection or model fitting is carried out by finding the \mathbf{c} that minimize χ^2 , with the other quantities held fixed. The values of \mathbf{c} that minimize χ^2 will be denoted by $\hat{\mathbf{c}} \equiv \{\hat{c}_l\}$; they are estimators of the harmonic amplitudes \mathbf{c} of the spatial correlations, which describe our particular realization of the Universe, as defined by (1). In contrast with Approach 1, which minimizes the variance of \hat{c}_l between different realizations of the Universe drawn from the Gaussian ensemble, this approach minimizes the overall mismatch χ^2 between the observed correlations in our Universe and the harmonic decomposition (1). (The Gaussian ensemble is employed to characterize how much mismatch will remain, on the average.)

To accomplish this minimization, take the partial derivative of (27) with respect to a particular $c_l \in \mathbf{c}$, and set it to zero:

$$\left. \frac{\partial \chi^2(\mathbf{c})}{\partial c_l} \right|_{\mathbf{c}=\hat{\mathbf{c}}} = 0. \quad (29)$$

For any given value of l , this results in a set of linear

equations for the estimators

$$\sum_{\hat{c}_{l'} \in \hat{\mathbf{c}}} F_{ll'} \hat{c}_{l'} = d_l, \quad (30)$$

where $F_{ll'}$ is defined in (12), and l ranges over the set of subscripts that appear in \mathbf{c} . To obtain (30), we combined terms, exploiting the fact that \mathbf{C}^{-1} is a symmetric matrix.

Note that the d_l , which were defined earlier in (7), are real, since $(\boldsymbol{\mu}_l \bar{\mathbf{H}})^t \mathbf{C}^{-1}$ annihilates the imaginary part of $\mathbf{Z}\mathbf{Z}$. This is a consequence of $\boldsymbol{\mu}_l$, $\bar{\mathbf{H}}$, and \mathbf{C}^{-1} all being real, which implies that

$$\bar{H}_{jk} (C^{-1})_{ab,cd}^{jk,\ell m} = \bar{H}_{-j,-k} (C^{-1})_{ab,cd}^{-j,-k,-\ell,-m}. \quad (31)$$

Thus,

$$\begin{aligned} & \sum_{jk} \sum_{\ell m} \bar{H}_{jk} (C^{-1})_{ab,cd}^{jk,\ell m} Z_c^\ell Z_d^m \\ &= \sum_{jk} \sum_{\ell m} \bar{H}_{-j,-k} (C^{-1})_{ab,cd}^{-j,-k,-\ell,-m} Z_c^{-\ell} Z_d^{-m} \\ &= \sum_{jk} \sum_{\ell m} \bar{H}_{jk} (C^{-1})_{ab,cd}^{jk,\ell m} Z_c^{-\ell} Z_d^{-m} \\ &= \sum_{jk} \sum_{\ell m} \bar{H}_{jk} (C^{-1})_{ab,cd}^{jk,\ell m} \Re(Z_c^\ell Z_d^m), \end{aligned} \quad (32)$$

where the first equality follows from changing the sign of the dummy summation variables j, k, ℓ, m ; the second equality follows from (31); and the last equality follows from the previous two lines and the definition of the real part of $\mathbf{Z}\mathbf{Z}$.

The number of linear equations (30) is the same as the number of c_l in the finite set \mathbf{c} . We can choose which ones

we wish to estimate, and are free to arbitrarily set some (e.g., \hat{c}_0 and/or \hat{c}_1) to zero (or other values) if desired. In any case, to arrive at a unique solution, the number of \hat{c}_l to be determined must equal the number of linearly independent equations. Let us use N_L to denote the number of \hat{c}_l that we wish to obtain, which is the order of the set \mathbf{c} . For example, if by fiat we constrain $\hat{c}_0 = \hat{c}_1 = 0$, then we would obtain values for $\hat{c}_2, \hat{c}_3, \dots, \hat{c}_{N_L+1}$. The solution for the \hat{c}_l are then given by

$$\hat{\mathbf{c}} = \mathbf{F}^{-1} \mathbf{d}, \quad (33)$$

where \mathbf{F}^{-1} is the matrix inverse (or pseudoinverse) of \mathbf{F} . Note that from here forward, we treat \mathbf{c} as a column vector of dimension N_L rather than as a set.

The application of \mathbf{F}^{-1} to \mathbf{d} can be thought of as “deconvolving” the response of the measurement process in order to extract the harmonic components c_l . In the context of map making, $\mathbf{F} \equiv F_{ll'}$ is called the “Fisher matrix” and the collection $\mathbf{d} \equiv d_l$ is called the “dirty map”, see [14, Sec. III.B]. The “clean map” $\hat{\mathbf{c}} \equiv \hat{c}_l$ is the end result of the deconvolution process. Indeed, it is easy to see that the “clean map” estimators $\hat{\mathbf{c}}$ are unbiased. This follows from $\langle d_l \rangle = u_l$, which we discussed in the sentences following (5), together with $u_l = \sum_{l'} F_{ll'} \langle c_{l'} \rangle$, which immediately follows from the definitions (8) and (12) of u_l and $F_{ll'}$.

The covariance of the estimators \hat{c}_l is easily calculated by first expressing it in terms of the covariance of the “dirty map” data d_l :

$$\begin{aligned} \sigma_{ll'}^2 &\equiv \langle \hat{c}_l \hat{c}_{l'} \rangle - \langle \hat{c}_l \rangle \langle \hat{c}_{l'} \rangle \\ &= \sum_{l_1} \sum_{l_2} (F^{-1})_{ll_1} (\langle d_{l_1} d_{l_2} \rangle - \langle d_{l_1} \rangle \langle d_{l_2} \rangle) (F^{-1})_{l_2 l'} \\ &= \sum_{l_1} \sum_{l_2} (F^{-1})_{ll_1} F_{l_1 l_2} (F^{-1})_{l_2 l'} \\ &= (F^{-1})_{ll'}, \end{aligned} \quad (34)$$

where we used (11) to obtain the third equality. Note that if $F_{ll'}$ is not invertible, then $(F^{-1})_{ll'}$ denotes its pseudoinverse, and the product $\mathbf{F}^{-1} \mathbf{F}$ is a rank- \mathbf{F} projector onto the nonnull space.

The variance of a particular \hat{c}_l estimator is obtained by setting $l = l'$ in (34):

$$\sigma_{\hat{c}_l}^2 \equiv \sigma_{ll}^2 = (F^{-1})_{ll}. \quad (35)$$

In analogy with Approach 1, we write this variance in the form

$$\sigma_{\hat{c}_l}^2 = \frac{\langle c_l \rangle^2}{(2L_{\text{eff}} + 1) N_{\text{freq}}} = (F^{-1})_{ll}, \quad (36)$$

where N_{freq} and $2L_{\text{eff}} + 1$ are functions of l . As noted for Approach 1, the division into the two factors is arbitrary. So we break this degeneracy by imposing the same two requirements as before. (See the discussion after (14).)

For requirement (i), we again consider the “crossover” frequency limit, where $N_{\text{freq}} \rightarrow N_{\text{cr}}$. As before, we find $\mathbf{F} \rightarrow 2N_{\text{freq}} \mathcal{G}$. But this time, we write this relation in terms of the diagonal components of the inverse matrices

$$(F^{-1})_{ll} \rightarrow \frac{(\mathcal{G}^{-1})_{ll}}{2N_{\text{freq}}} \quad \text{for } l \geq 2, \quad (37)$$

where \mathcal{G}^{-1} is the pseudoinverse of \mathcal{G} . Substituting this limiting expression for $(F^{-1})_{ll}$ into the rhs of (36) implies that

$$2L_{\text{eff}} + 1 \equiv \frac{2\langle c_l \rangle^2}{(\mathcal{G}^{-1})_{ll}}. \quad (38)$$

As we argued for Approach 1, this relation must always hold as a consequence of requirement (ii). It then follows from (36) that

$$N_{\text{freq}} \equiv \frac{1}{2} \frac{(\mathcal{G}^{-1})_{ll}}{(F^{-1})_{ll}}. \quad (39)$$

As we saw for Approach 1, the effective number of harmonic degrees of freedom $2L_{\text{eff}} + 1$ simplifies when there are many pulsars uniformly distributed on the sky. In this limit (38) gives

$$2L_{\text{eff}} + 1 \equiv \frac{2\langle c_l \rangle^2}{(\mathcal{G}^{-1})_{ll}} \rightarrow 2\langle c_l \rangle^2 \mathcal{G}_{ll} \rightarrow 2l + 1 \quad \text{for } l \geq 2, \quad (40)$$

as a consequence of (22). This is precisely the number of degrees of freedom associated with harmonic index l .

Table I shows values of $2L_{\text{eff}} + 1$ computed using (38) (with $N_L = 16$) for several real and fictional PTAs. We note that when the number of pulsars is large, the values of $2L_{\text{eff}} + 1$ are similar for both approaches. We expect that $2L_{\text{eff}} + 1$ should satisfy $2L_{\text{eff}} + 1 \leq 2l + 1$, but have not been able to prove this. We would have expected that adding pulsars to an array always increases $2L_{\text{eff}} + 1$, but we have been unable to prove this and note that numerical experiments indicate that it is not the case for Approach 1, though there it appears that the sum over l of $2L_{\text{eff}} + 1$ always increases.

Conclusion.— There is a substantial literature on the harmonic approach to PTAs (see [11] and references therein). These represent the mean correlations between pulsars as a sum of Legendre polynomials of the cosine of the pulsar-pair separation angle. The coefficients in that expansion characterize the correlations.

Here, we have shown two ways to estimate these coefficients from measured redshift or timing-residual measurements. The first approach minimizes the expected variance away from the mean, for a single coefficient “in isolation”. The second approach minimizes the square of the mean deviation away from the expected value, where the measure on the quadratic form is constructed in the same way as for a conventional χ^2 statistic. Of greatest

interest to us is not the estimators themselves but rather their variances.

In both cases, the variance is written as a ratio, where the numerator $\langle c_l \rangle^2$ is the square of the expected value, and the denominator is an effective number of degrees of freedom. This denominator, in turn, is the product of an effective number of angular degrees of freedom and an effective number of frequency degrees of freedom. Both of these depend upon l , but the effective number of angular degrees of freedom is determined entirely by the geometry of the PTA, whereas the effective number of frequency bins depends upon the spectral properties of the GWB and pulsar noise. The corresponding formulas for first approach are given in (14), (18) and (19), and for the second approach in (36) (38) and (39).

The ‘‘harmonic-space’’ analysis done here closely parallels a corresponding ‘‘position-space’’ analysis done in [7], and shares many similar features. Both construct frequency-weighted estimators of the HD correlation. In comparison with the ‘‘white, zero-lag’’ estimators of the HD correlation used in [8, 13], these permit a further reduction in the variance. Indeed, by increasing the effective number of signal-dominated frequency bins, the effects of cosmic variance can in principle be reduced as much as desired. Such an increase can be achieved either by adding additional ‘‘quiet’’ pulsars to the PTA, or alternatively, by increasing the observation time. Similar conclusions have been reached in [15].

We believe that applying these approaches to PTA posteriors will provide a useful tool to characterize and quantify the HD correlations and their deviations from the HD curve.

* bruce.allen@aei.mpg.de

† joseph.romano@utrgv.edu

- [1] R. W. Hellings and G. S. Downs, Upper limits on the isotropic gravitational radiation background from pulsar timing analysis, *Astrophys. J.* **265**, L39 (1983).
 [2] J. Antoniadis *et al.* (EPTA and InPTA Collaborations), The second data release from the European Pulsar Tim-

- ing Array: III. Search for gravitational wave signals, *Astronomy & Astrophysics* **678**, A50 (2023).
 [3] G. Agazie *et al.* (NANOGrav Collaboration), The NANOGrav 15 yr Data Set: Evidence for a Gravitational-wave Background, *The Astrophysical Journal Letters* **951**, L8 (2023).
 [4] D. J. Reardon *et al.* (PPTA Collaboration), Search for an Isotropic Gravitational-wave Background with the Parkes Pulsar Timing Array, *The Astrophysical Journal Letters* **951**, L6 (2023).
 [5] H. Xu *et al.* (CPTA Collaboration), Searching for the Nano-Hertz Stochastic Gravitational Wave Background with the Chinese Pulsar Timing Array Data Release I, *Research in Astronomy and Astrophysics* **23**, 075024 (2023).
 [6] M. T. Miles *et al.*, The MeerKAT Pulsar Timing Array: the first search for gravitational waves with the MeerKAT radio telescope, *Monthly Notices of the Royal Astronomical Society* **536**, 1489 (2024).
 [7] B. Allen and J. D. Romano, Optimal reconstruction of the Hellings and Downs correlation (2024), arXiv:2407.10968 [gr-qc].
 [8] B. Allen and J. D. Romano, Hellings and Downs correlation of an arbitrary set of pulsars, *Phys. Rev. D* **108**, 043026 (2023).
 [9] J. Gair, J. D. Romano, S. Taylor, and C. M. F. Mingarelli, Mapping gravitational-wave backgrounds using methods from CMB analysis: Application to pulsar timing arrays, *Phys. Rev. D* **90**, 082001 (2014).
 [10] E. Roebber and G. Holder, Harmonic space analysis of pulsar timing array redshift maps, *Astrophys. J.* **835**, 21 (2017).
 [11] B. Allen, Pulsar timing array harmonic analysis and source angular correlations, *Phys. Rev. D* **110**, 043043 (2024).
 [12] J. D. Romano and B. Allen, Answers to frequently asked questions about the pulsar timing array Hellings and Downs curve, *Classical Quantum Gravity* **41**, 175008 (2024).
 [13] B. Allen, Variance of the Hellings-Downs correlation, *Phys. Rev. D* **107**, 043018 (2023).
 [14] E. Thrane, S. Ballmer, J. D. Romano, S. Mitra, D. Talukder, S. Bose, and V. Mandic, Probing the anisotropies of a stochastic gravitational-wave background using a network of ground-based laser interferometers, *Phys. Rev. D* **80**, 122002 (2009).
 [15] C. Pitrou and G. Cusin, Mitigating cosmic variance in the Hellings-Downs curve: a Cosmic Microwave Background analogy (2024), arXiv:2412.12073 [gr-qc].